PRAMANA — journal of physics

Vol. 79, No. 1
July 2012
pp. 125–136

Electron transport in wurtzite InN

F M ABOU EL-ELA* and B M EL-ASSY

Department of Physics, Faculty of Girls, Ain Shams University, Heliopolis, Cairo, Egypt
*Corresponding author. E-mail: fadlaeg@yahoo.com

MS received 4 July 2011; revised 7 January 2012; accepted 8 February 2012

Abstract. Using ensemble Monte Carlo simulation technique, we have calculated the transport properties of InN such as the drift velocity, the drift mobility, the average electron, energy relaxation times and momentum relaxation times at high electric field. The scattering mechanisms included are polar optical phonon, ionized impurity, acoustic phonon and intervalley phonon. It is found that the maximum peak velocity only occurs when the electric field is increased to a value above a certain critical field. This critical field is strongly dependent on InN parameters. The steady-state transport parameters are in fair agreement with other recent calculations.

Keywords. InN transport; mobility; energy and momentum relaxation; impurity scattering.

PACS No. 72.20.Ht

1. Introduction

Group III-nitrides are usually considered as wide-band-gap materials that have applications in ultraviolet/blue/green light-emitting diodes and lasers [1]. However, recent experimental and theoretical investigations have provided convincing evidence that the band gap of wurtzite InN is (about 0.7 eV) [2–6] much smaller than the (1.89–1.5) eV band gap [6,7] widely accepted in the past to interpret experimental data [1] and to fit empirical pseudopotentials for modelling InN and related alloy properties [8]. If InN indeed has a band gap less than 1.0 eV, which is even smaller than that for InP (1.4 eV), then InN and its III-nitride alloys can also be suitable for low band-gap devices such as future generation solar cell because the nitride alloys can cover the whole solar spectrum range.

An understanding of the electron transport in InN is necessary to improve InN semiconductor-based devices. Transport properties of InN at both steady state and transient state have been discussed extensively over the years [9–15]. Uncertainty in material band parameters remain a key source of ambiguity in the analysis of electron transport properties. Monte Carlo transport properties [12–15] are based on 0.7 eV band gap and band structure parameters published in [16].

DOI: 10.1007/s12043-012-0294-5; ***e*Publication: 23 June 2012**

Table 1. The material parameters of bulk wurtzite InN used for simulations [11].

Mass density (g/cm^3)	6.81
Longitudinal sound velocity (cm/s)	6.24×10^5
Acoustic deformation potential (eV)	7.10
Static dielectric constant	15.30
High-frequency dielectric constant	8.40
Optical phonon energy (eV)	0.089
Intervalley deformation potentials (eV/cm)	10^9
Intervalley phonon energies (eV)	0.089
Piezoelectric constant (C/cm^2)	3.75×10^{-5}

We apply the ensemble Monte Carlo method to investigate the electron transport in bulk wurtzite InN based on the refined band structure used in [12–15].

Monte Carlo simulation method is a technique of simulation motion of many carriers in k-space. It allows one to know exactly the average electron velocity, the average electron mobility, the average electron energy and many other parameters. It is a more accurate and exact method, but it requires running a computer program whenever a new condition arises.

In this work, we used the ensemble Monte Carlo technique [17–20] to evaluate the transport properties of InN at high electric fields. Tables 1 and 2 show the selected parameters of InN. In our calculation, the band structure of wurtzite InN is approximated by the three lowest conduction band minima Γ_1, Γ_3 and M-L valleys. Parameters such as effective masses m^*, nonparabolicity factors α for the valleys, and valley separation energies have been extracted from a conduction band structure recently calculated by the empirical pseudopotential method [16]. The satellite valleys Γ_3 and M-L are assumed to be parabolic (i.e., $\alpha = 0.0$), while the main Γ_1 valley is isotropic nonparabolic.

In this work, the scattering rates of our scattering mechanisms are presented and analysed in §3. After that, the number of transport parameters associated with the bulk wurtzite InN is discussed.

Table 2. The valley parameters corresponding to the bulk wurtzite InN. The values of the model parameters have been obtained by fitting the theoretical conduction band dispersion data from ref. [16].

Valley number	1	2	3
Valley location	Γ_1	Γ_3	L-M
Valley degeneracy	1	1	6
Effective mass	0.04	0.25	1.00
Intervalley energy separation (eV)	–	1.775	2.709
Energy gap (eV)	0.7	2.475	3.409
Nonparabolicity (eV^{-1})	1.43	0.0	0.0

2. Parameter selections for bulk wurtzite InN

The material parameters used for our simulations are tabulated in table 1. These parameters are selected from [16] and originally from Foutz *et al* [11].

3. Scattering mechanisms

This section lists the most important types of different phonons scattering rates and ionized impurity scattering used in the Monte Carlo method, assuming nonparabolic bands at the lattice temperature T.

For more details of these scattering rates, the reader is referred to [17–22].

3.1 *Scattering rates of acoustic phonons*

The interaction of the acoustic phonon is due to the deformation potential and is given by

$$\Gamma_{\mathrm{ac}}(E) = \frac{(2m^*)^{3/2} k_{\mathrm{B}} T}{2\pi\rho s_{\mathrm{v}}^2 \hbar^4} \Xi_a^2 \gamma^{1/2}(E)(1+2\alpha E) F_a(E), \tag{1}$$

where

$$\gamma(E) = E(1+\alpha E) \quad \text{and} \quad F_a(E) = \frac{(1+\alpha E)^2 + 1/3(\alpha E)^2}{(1+2\alpha E)^2}$$

Ξ_a, ρ and s_{v} respectively represent the acoustic deformation potential, the specific mass density of the crystal and the sound velocity and α is the nonparabolicity factor.

3.2 *Scattering rates of polar optical phonons*

The scattering rate due to the polar optical phonon is evaluated as

$$\begin{aligned}\Gamma_{\mathrm{po}}(E) = {} & \frac{e^2 m^{*1/2} \hbar\omega_{\mathrm{po}}}{4\sqrt{2}\pi\varepsilon_0\hbar^2} \left(\frac{1}{\varepsilon_\infty} - \frac{1}{\varepsilon_{\mathrm{s}}}\right) \frac{1+2\alpha E'}{\gamma^{1/2}(E)} F_0(E, E') \\ & \times \left(N_{\mathrm{po}} + 1/2 \pm 1/2\right), \end{aligned} \tag{2}$$

where N_{po} is the optical phonon occupation number, which is given by Bose–Einstein statistics. The $\pm$ sign refers to phonon emission or absorption respectively. $\hbar\omega_{\mathrm{po}}$, ε_{s}, ε_∞ and ε_0 represent the energy of polar optical phonon, the relative static dielectric constant, the high frequency dielectric constant and the permittivity of free space, respectively.

In the above equation, we use the following notation:

$$\begin{aligned} &\gamma(E') = E'(1+\alpha E') \\ &F_0(E, E') = C^{-1}\left[A \ \ln\left|\frac{\gamma^{1/2}(E) + \gamma^{1/2}(E')}{\gamma^{1/2}(E) - \gamma^{1/2}(E')}\right| + B\right] \\ &A = [2(1+\alpha E)(1+\alpha E') + \alpha(\gamma(E) + \gamma(E'))]^2 \\ &B = -2\alpha\gamma^{1/2}(E)\gamma^{1/2}(E') \\ &\quad \times [4(1+\alpha E)(1+\alpha E') + \alpha(\gamma(E) + \gamma(E')))] \\ &C = 4(1+\alpha E)(1+\alpha E')(1+2\alpha E)(1+2\alpha E'). \end{aligned} \tag{3}$$

3.3 *Scattering rates of equivalent intervally phonons*

We shall consider equivalent intervalley phonon scattering in the Γ_3 and M-L bands only. The intervalley scattering rate for all possible transitions between equivalent valleys is given by

$$\Gamma_{\mathrm{e}}(E) = (Z_{\mathrm{e}} - 1)\frac{m^{*3/2} D_{\mathrm{e}}^2}{\sqrt{2}\pi\hbar^3\rho\omega_{\mathrm{e}}}\gamma^{1/2}(E')(1 + 2\alpha E') \times (N_{\mathrm{e}} + 1/2 \pm 1/2), \tag{4}$$

where ω_{e} is the equivalent intervalley phonon frequency, D_{e} is the deformation potential for the equivalent intervalley scattering, Z_{e} is the number of equivalent valleys and N_{e} is the equivalent intervalley phonon occupation number, which is given by Bose–Einstein statistics.

3.4 *Scattering rates of nonequivalent intervalley phonons*

In high electric fields, the electron energy of InN may become sufficiently high, and so electrons scatter into the Γ_3 and M-L valleys. The intervalley scattering rate between non-equivalent valleys is given by

$$\Gamma_{ij}(E) = Z_j\frac{m_j^{*3/2} D_{ij}^2}{\sqrt{2}\pi\hbar^3\rho\omega_{ij}}\gamma^{1/2}(E')(1 + 2\alpha E') \times (N_{ij} + 1/2 \pm 1/2), \tag{5}$$

where ω_{ij} is the intervalley phonon frequency, D_{ij} is the deformation potential for non-equivalent intervalley scattering, Z_j is the number of valleys of type j and N_{ij} is the intervalley phonon occupation number, which is also given by Bose–Einstein statistics. The electron energy is measured from the minimum of the valley which are situated at energies Δ_i and Δ_j for valleys i and j, respectively, while $\hbar\omega_{ij}$ is the energy of the phonon involved.

$$E' = E_i - \Delta_j + \Delta_i + \hbar\omega_{ij}, \quad \text{phonon absorption},$$
$$E' = E_i - \Delta_j + \Delta_i + \hbar\omega_{ij}, \quad \text{phonon emission}.$$

3.5 *Scattering rates of ionizied impurity*

The most popular studies for handling the scattering by ionized impurities in Monte Carlo calculation are done by Brooks and Herring (BH) [21] and Conwell and Weisskopf (CW) [22]. The CW model was chosen in our study because it covers a greater range of ionized concentration and compensation ratios than BH model. We consider InN to be uncompensated and all donors to be ionized.

The CW scattering rate for ionized impurity scattering was given in CW approach [18,19,22] as

$$\Gamma_{\mathrm{CW}}(E) = \pi N_{\mathrm{I}} Z^2 b^2 \left(\frac{2}{m^*}\right)^{1/2} \frac{E^2(1 + 2\alpha E)}{\gamma^{3/2}(E)}, \tag{6}$$

where N_{I} and Z are the impurity concentration and charge of the impurity.

In CW approach, an unscreened bare Coulomb potential is assumed, which cuts off at mean distance between impurities, b, given by

$$b = \left[\frac{3}{4\pi N_{\mathrm{I}}}\right]^{1/3}.$$

4. Results and discussion

4.1 *Effect of scattering mechanisms on the electron energy in InN*

We shall discuss in this section the effect of scattering mechanisms on the electron energy. The scattering mechanisms included in our work are polar optical phonon scattering (POP), ionized impurity scattering (CW), intervalley phonon scattering (IVP) and acoustic deformation potential scattering (AC).

Figures 1 and 2 illustrate the computed scattering rates for phonons in the Γ_1 valley in InN. The principle source of scattering is due to optical phonons either through polar interaction or through intervalley deformation potential mechanism. The other scattering mechanisms in figure 2, which are the ionized impurity scattering and the acoustic deformation potential scattering, do not remove energy from the electron ensemble: they are elastic scattering mechanisms. It is seen that the acoustic scattering rate and ionized impurity scattering rate are very small compared to polar optical phonon scattering rate.

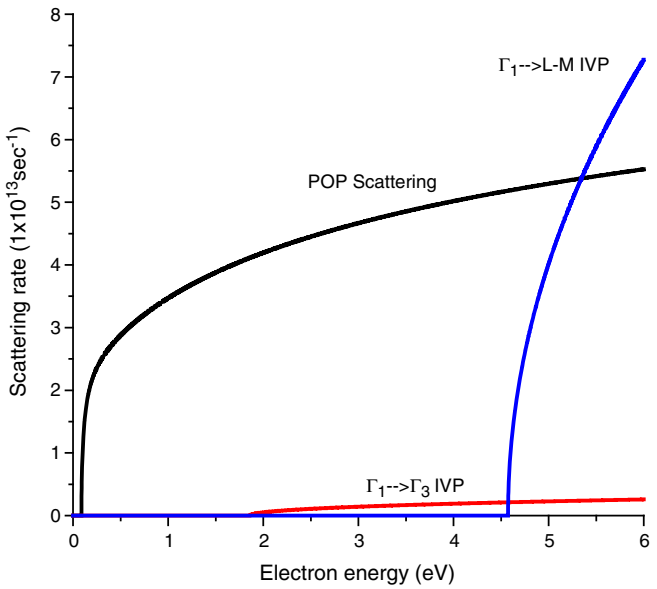

Figure 1. Scattering rate as a function of electron energy due to POP and intervalley scattering mechanism.

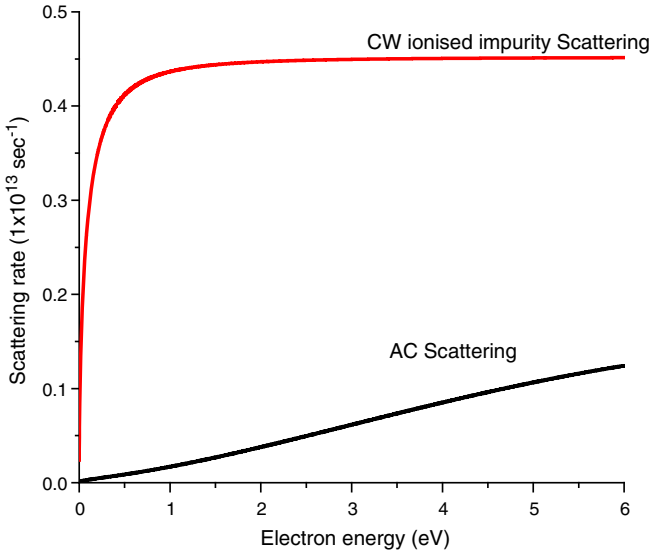

Figure 2. Scattering rate as a function of electron energy due to the ionized impurity scattering and acoustic deformation potential scattering at Γ_1-valley in InN.

In figure 1, the POP scattering and intervalley phonon scattering (IVP) include both emission and absorption scattering rates. The POP scattering starts at low energies that electrons acquire from the electric field. After that, the POP scattering is strongly modified by taking into account the strong nonparabolicity in a way that the scattering rate becomes an increasing function with electron energy. When electron energy increases, electrons will acquire enough energy in order to transfer into the upper valleys and intervalley scattering will appear and this becomes the dominant scattering mechanism. The effective mass of electrons will increase gradually when the electric field increases and then the saturation value and an energy balance is re-established.

4.2 *Steady-state electron transport parameters within the bulk wurtzite InN*

The velocity–field characteristics associated with InN is presented in figure 3. The crystal temperature is set to 300 K and the doping concentration to 10^{16} cm^{-3}. The higher peak velocity of 61×10^6 cm/s occurs at 40×10^3 V/cm. After that, the electron drift velocity decreases until it reaches its saturation value at high applied electric fields.

Now we shall discuss the results at low applied electric fields corresponding to a field less than 40×10^3 V/cm, which is an ohmic region that is followed by a negative differential resistance (NDR). At the beginning all the electrons occupy the central Γ_1 valley which is a nonparabolic band with 1.43 (see table 2). After increasing the electric field, the average electron velocity remains relatively low due to the POP scattering, with most of the energy gained from the applied electric field being transferred into the lattice through this type of scattering. Due to the nonparabolicity of the central valley, the POP scattering

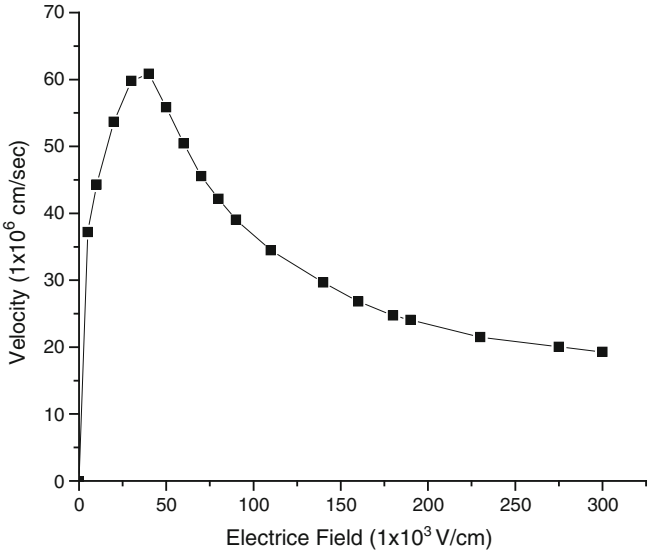

Figure 3. The velocity–field characteristics of InN.

increases with the increase in electric field until the average velocity reaches a value at which the electrons overcome the POP scattering and reaches its peak value. The peak velocity occurs at an electric field where most electrons still reside in the central valley and after that they begin to jump to the upper valleys. The intervalley scattering continues and electrons become slower due to the increase of the effective mass of electron in the upper valley. Finally, at high applied electric fields, the average drift velocity reaches its saturation value.

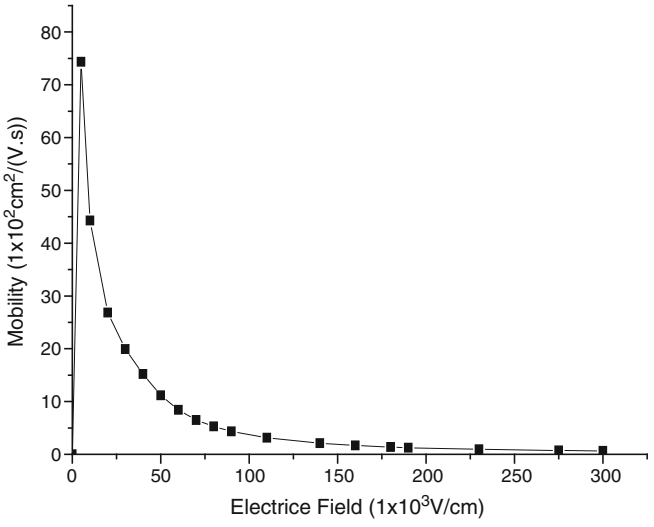

Figure 4. The average drift mobility as a function of electric field.

In figure 4, the average electron drift mobility has its maximum value at very low values of the electric field due to the smallest effective mass for the electrons in the central valley. The negative differential mobility (NDM) is observed by increasing the electric fields due to intervalley transfer mechanism. A linear low-field electron drift velocity dependence on the applied electric field $v_d = \mu E$, applies in this regime. At high electric field, the average electron drift mobility reaches low values due to the increase of effective mass of the electron in higher valleys.

If we examine the electron energy as a function of the applied electric field (figure 5), we see that there is a sudden increase at around 40×10^3 V/cm. When the applied electric field is less than 40×10^3 V/cm, the energy that the electrons gain from the applied electric field is lost through polar optical phonon scattering. The scattering rate increases with the increase of the electric field until the electrons get enough energy to transfer to the higher valleys and at this point a sudden increase is observed. When electron energy is around 1.775 eV, electrons can transfer to Γ_3 valley whereas if it is around 2.709 eV, they can transfer to M-L valley. At higher values of electric field, electron energy reaches its saturation value.

We can see in figure 6 the effective mass of the electron in the central valley as a function of the applied electric field. Electrons which occupy the Γ_1 valley have an effective mass around 0.04. By increasing the electric field, the electrons jump into the higher valleys and their effective mass increases until it reaches its saturation value.

Figure 7 gives us the fractional number of the three lower valleys as a function of the applied electric field. First, we can see that all electrons occupy the Γ_1 valley until they begin to transfer to the Γ_3 valley around 40×10^3 V/cm. By increasing the electric field, electrons begin to transfer to the M-L valley until each valley is occupied by maximum electrons and the saturation is established.

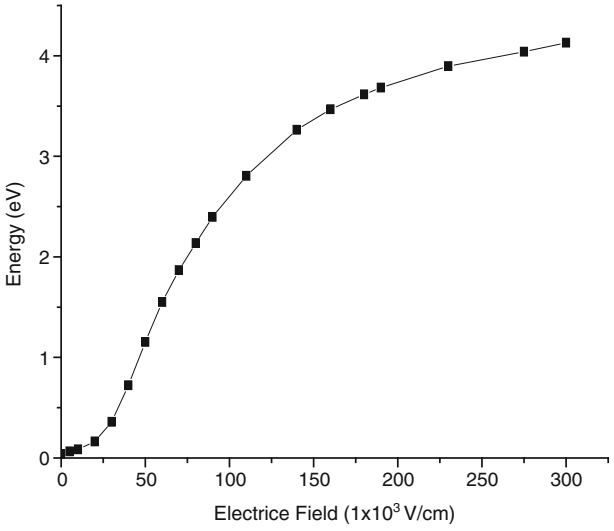

Figure 5. The average electron energy as a function of electric field.

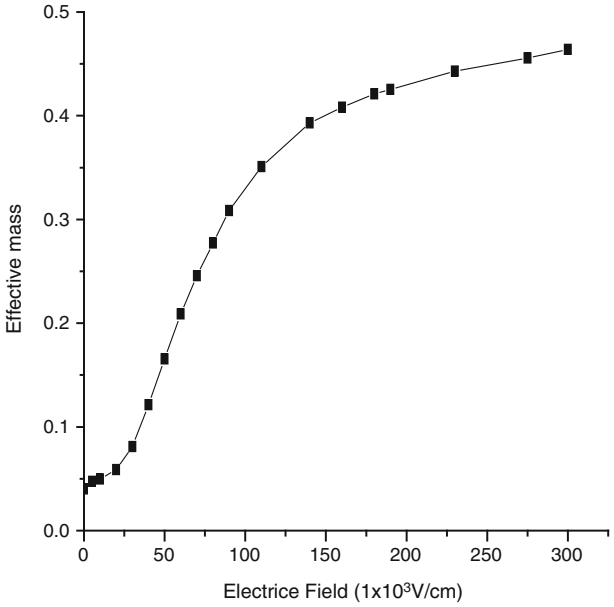

Figure 6. The effective mass of the electrons in 0-valley as a function of the electric field.

The momentum and the energy balance equations for an electron at high electric field (F) are given by eqs (7) and (8) [11] respectively.

$$\frac{\mathrm{d}(m^*V)}{\mathrm{d}t} = -eF - \frac{m^*V}{\tau_\mathrm{m}}, \tag{7}$$

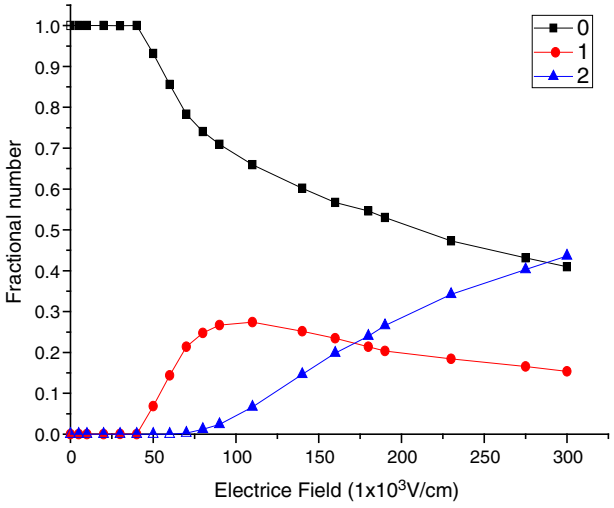

Figure 7. The fractional number of the three lower valleys as a function of the applied electric field.

$$\frac{\mathrm{d}E}{\mathrm{d}t} = -eVF - \frac{(E - E_0)}{\tau_\mathrm{e}}, \tag{8}$$

where τ_m is the effective momentum relaxation time, τ_e is the effective energy relaxation time, $E_0 = (3/2)K_\mathrm{B}T$, T is the lattice temperature, K_B is the Boltzmann constant. The energy-dependent effective mass m^* is an average of the effective mass over the ensemble, the effective mass being dependent on the valley the electron occupies. m^*, τ_m and τ_e are determined by the steady-state Monte Carlo calculation using the equations

$$m^* = m_0^*(1 + 2\alpha E),$$

$$\tau_\mathrm{m} = \frac{m^* V}{qF}$$

and

$$\tau_\mathrm{e} = \frac{E - E_0}{qVF},$$

where E is the steady-state average electron energy and V is the steady-state electron average drift velocity as a function of electric field.

In most of the semiconductors, the energy relaxation time (τ_e) is slower than the momentum relaxation time (τ_m) so that the electrons exhibit the phenomenon of velocity overshoot. In the absence of intervalley transfer, the electrons would relax its velocity over a long time. The intervention of intervalley scattering relaxes the velocity much quicker, due to the large effective mass and scattering rates in the upper valley in comparison to the lower valley.

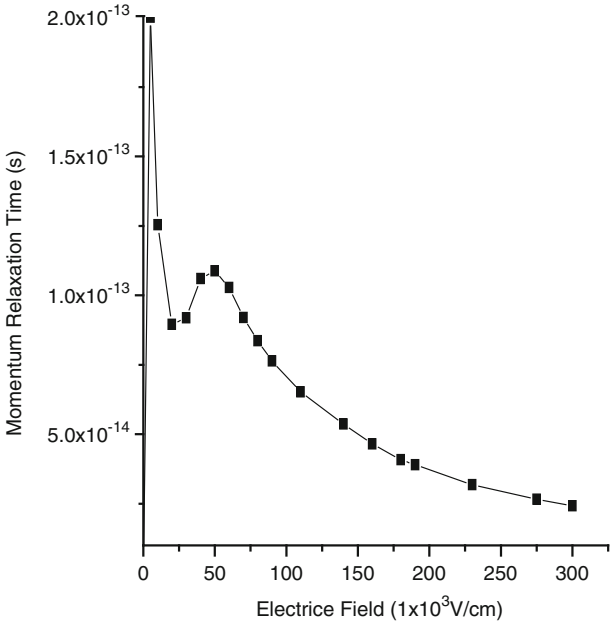

Figure 8. The momentum relaxation time as a function of the applied electric field.

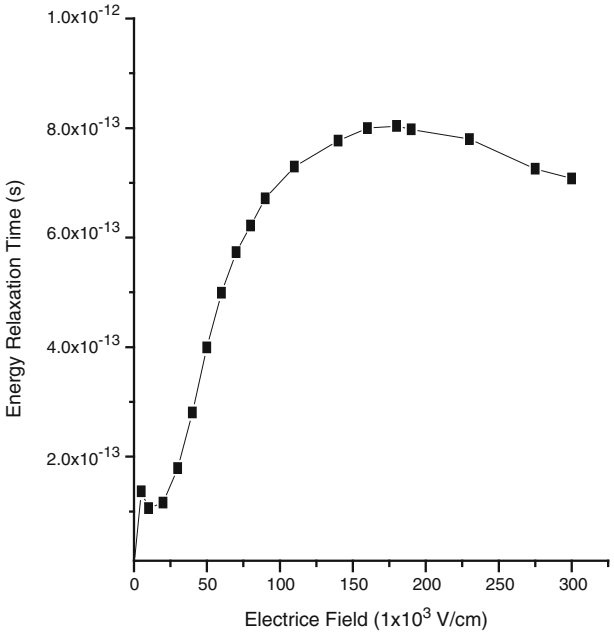

Figure 9. The energy relaxation time as a function of the applied electric field.

Figures 8 and 9 show the momentum relaxation time and the energy relaxation time vs. electric fields in InN. The momentum relaxation time decreases as electric field increases at applied electric fields corresponding to a field higher than 40×10^3 V/cm, which is a negative differential resistance (NDR) region due to intervalley scattering to higher Γ_3 and M-L valleys. On the contrary, the energy relaxation time increases for the same reasons which were already mentioned.

5. Conclusions

In this work we have investigated the steady-state properties in bulk wurtzite InN using the ensemble Monte Carlo technique. The main emphasis is given to the origin of the negative differential mobility for the steady-state transport. We found that the nonparabolicity of the central Γ_1 valley strongly influences the transport properties in InN. The dominant POP scattering rate, however, becomes an increasing function of electron energy and, as a result, the peak drift velocity occurs at considerably lower electric fields compared to the onset of intervalley transfer. At higher electric fields, the satellite valleys with heavier effective mass also contribute to the NDM effect. We also reviewed analyses on the scattering rates of a number of scattering mechanisms on the electron energy and observed the high values of POP scattering rate. For that, the electron velocity in the central valley saturates or even decreases at energies well below the threshold energy of the electron transfer to the satellite valleys with heavier effective mass.

References

[1] H Morkoç, *Nitride semiconductors and devices* (Springer, New York, 1999)
[2] V Y Davydov *et al*, *Phys. Status Solidi* **B230**, R4 (2002)
[3] J Wu *et al*, *Appl. Phys. Lett.* **80**, 3967 (2002)
[4] J Wu *et al*, *Phys. Rev*. **B66**, 201403 (2002)
[5] T Matsuoka, H Okamoto, M Nakao, H Harima and E Kurimoto, *Appl. Phys. Lett.* **81**, 1246 (2002)
[6] T Inushima, V Mamutin, V Vekshin, S Ivanov, T Sakon, M Motokawa and S Ohoya, *J. Crystal Growth* **227/228**, 481 (2001)
[7] T Tansley and C Foley, *J. Appl. Phys.* **59**, 3241 (1986)
[8] *Semiconductors: Data handbook* edited by O Madelung (Springer, Berlin, 2004)
[9] S K O'Leary, B E Foutz, M S Shur, U V Bhapkar and L F Eastman, *J. Appl. Phys.* **83**, 826 (1998)
[10] E Bellotti, B K Doshi, K F Brennan, J D Albrecht and P P Ruden, *J. Appl. Phys.* **85**, 916 (1999)
[11] B E Foutz, S K O'Leary, M S Shur and L F Eastman, *J. Appl. Phys.* **85**, 7727 (1999)
[12] C Bulutay and B K Ridley, *Superlattices Microstruct.* **36**, 465 (2004)
[13] V M Polyakov, F Schwierz, D Fritsch and H Schmidt, *Phys. Status Solidi* **C3**, 598 (2006)
[14] V M Polyakova and F Schwierz, *J. Appl. Phys. Lett.* **88**, 032101 (2006)
[15] V M Polyakova and F Schwierz, *J. Appl. Phys.* **99**, 113705 (2006)
[16] D Fritsch, H Schmidt and M Grundmann, *Phys. Rev*. **B69**, 165204 (2004)
[17] W Fawcett, A D Boardman and S Swain, *J. Phys. Chem. Sol.* **31**, 1963 (1970)
[18] C Jacoboni and L Reggiani, *Rev. Mod. Phys.* **55(3)**, 645 (1983)
[19] *The Monte Carlo method for semiconductor device simulation* edited by Carlo Jacoboni and Paolo Lugli (Springer-Verlag/Wien, 1989)
[20] F M Abou El-Ela, *Monte Carlo study of transport in GaAs*, Ph.D. Thesis (Essex University, England, 1989)
[21] H Brooks and C Herring, *Phys. Rev*. **83**, 879 (1951)
[22] E Conwell and V P Weisskopf, *Phys. Rev*. **77**, 388 (1950)